

# Mediator–Antisolvent Strategy to Stabilize All-Inorganic CsPbI<sub>3</sub> for Perovskite Solar Cells with Efficiency Exceeding 16%

Ting Zhang, Feng Wang,\* Hao Chen, Long Ji, Yafei Wang, Chun Li, Markus B. Raschke, and Shibin Li\*

Cite This: *ACS Energy Lett.* 2020, 5, 1619–1627

Read Online

ACCESS |



Metrics &amp; More

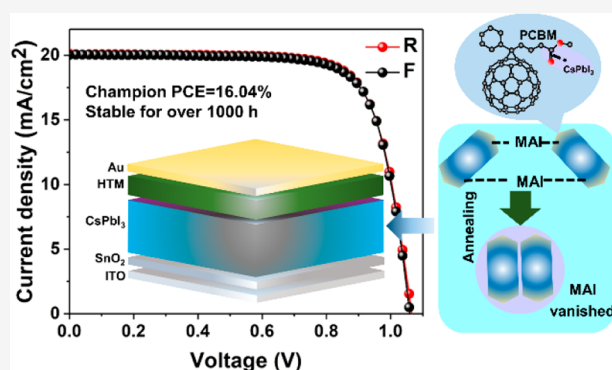


Article Recommendations



Supporting Information

**ABSTRACT:** All-inorganic cesium lead triiodide (CsPbI<sub>3</sub>) perovskites have attracted much attention because of their intrinsic chemical stability and suitable bandgap for photovoltaic applications. However, simple methods to synthesize pure CsPbI<sub>3</sub> have been limited. Here, we develop a new mediator–antisolvent strategy (MAS) combining phenyl-C61-butyric acid methyl ester (PCBM) blended chlorobenzene (CBZ) antisolvent and methylammonium iodide (MAI) mediator to synthesize high-quality and stable black-phase CsPbI<sub>3</sub> perovskite films. The crystallization process is altered by the blended antisolvent, leading to a smaller crystallite of the perovskite with improved stability. The small amount of MAI acts as mediator and further improves the quality of the CsPbI<sub>3</sub> films in morphology and photoelectronic properties. Finally, the power conversion efficiency of CsPbI<sub>3</sub> perovskite solar cells prepared by the strategy significantly increases to a value of  $\geq 16\%$  with good reproducibility. Moreover, the devices retain 95% of their original efficiency over 1000 h.



During the past decade, halide perovskites have gained great attention and have been considered as a promising material for next-generation photovoltaics. Since the emergence of perovskite-based solar cells (PSCs) in 2009,<sup>1</sup> certified power conversion efficiencies (PCEs) of organic–inorganic halide PSCs have rapidly increased to 25.2%.<sup>2</sup> Although continuous progress in improving efficiency is being made, there are hurdles for their large-scale deployment because of the unsatisfactory long-term stability of hybrid perovskites owing to the degradation and volatilization of organic groups, e.g., methylammonium (MA<sup>+</sup>) and formamidinium (FA<sup>+</sup>) cations.<sup>3–5</sup> For this reason, all-inorganic perovskites have attracted intensive research interest recently because of their intrinsic chemical stability.<sup>6–9</sup>

Among these cesium lead halide perovskites CsPbX<sub>3</sub> (X = Cl, Br, and I), cesium lead iodide (CsPbI<sub>3</sub>) possesses the most suitable bandgap ( $\sim 1.7$  eV) for photovoltaic applications. It not only is suitable as light-harvesting material in high performance single-junction PSCs but also is ideal for the top cell of perovskite/silicon tandem solar cells.<sup>6</sup> However, CsPbI<sub>3</sub> is metastable in photoactive black phase ( $\alpha$ -CsPbI<sub>3</sub>,  $\beta$ -CsPbI<sub>3</sub>, and  $\gamma$ -CsPbI<sub>3</sub>) and easily degrades to nonperovskite  $\delta$ -phase (yellow phase) because of the undesired tolerance factor.<sup>10</sup> When exposed to humidity, Cs ions get displaced

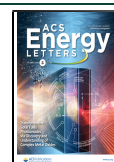
from their original lattice positions to accommodate H<sub>2</sub>O into the CsPbI<sub>3</sub> lattice, which causes the distortion of the corner-sharing [PbI<sub>6</sub>]<sup>4-</sup> octahedron frameworks and leads to the phase transition into the photoinactive  $\delta$ -CsPbI<sub>3</sub>.<sup>11,12</sup> Therefore, numerous efforts have been made to stabilize the black phase of CsPbI<sub>3</sub>, primarily by introducing HI or HPbI<sub>3</sub> in perovskite precursor,<sup>7,13–17</sup> quantum dots/nanocrystals effects,<sup>18–21</sup> tuning tolerance factor by element substitution,<sup>22–25</sup> and 2D/3D surface modification.<sup>14,26,27</sup>

Adding HI or HPbI<sub>3</sub> in the precursor is reported to stabilize the black-phase perovskites at a lower temperature, which is ascribed to the extra strain introduced.<sup>13–17</sup> In contrast, other work suggests that the reported all-inorganic black-phase CsPbI<sub>3</sub> perovskites are in fact a mixed-cation perovskite Cs<sub>1-x</sub>DMA<sub>x</sub>PbI<sub>3</sub> (DMA = dimethylammonium, (CH<sub>3</sub>)<sub>2</sub>NH<sub>2</sub><sup>+</sup>) containing a substantial portion of DMA cations.<sup>28</sup> DMA, an organic component, may impair the superior thermal stability

Received: March 2, 2020

Accepted: April 21, 2020

Published: April 21, 2020



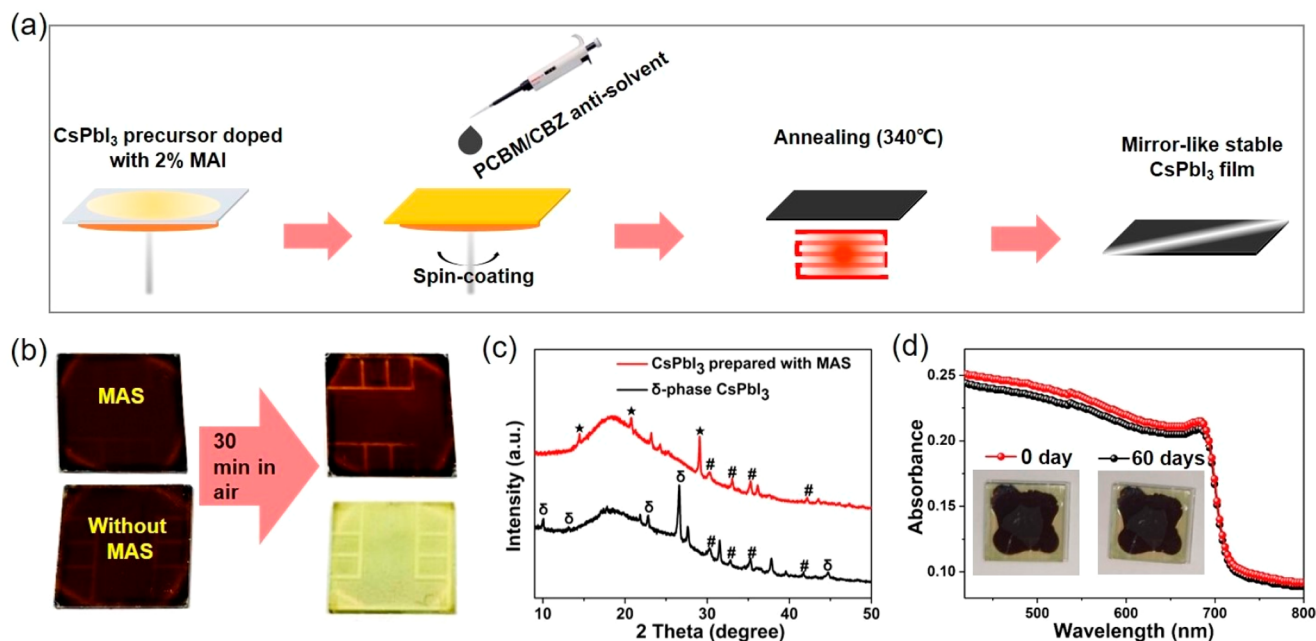


**Figure 1.** MAS for CsPbI<sub>3</sub> perovskite deposition. (a) Schematics of MAS. (b) Optical images of fresh and aged (kept in ambient air for 30 min) CsPbI<sub>3</sub> films prepared by MAS and conventional one-step method. (c) XRD patterns of black-phase CsPbI<sub>3</sub> films prepared with MAS and degraded CsPbI<sub>3</sub> films prepared with conventional one-step method. Both films were encapsulated with Kapton tape. “#” denotes diffraction peaks of ITO. “★” denotes diffraction peaks of black-phase CsPbI<sub>3</sub>. (d) Absorption spectra of encapsulated CsPbI<sub>3</sub> films prepared with MAS kept in ambient air with 70%–90% relative humidity for 2 months. Insets are the photos of encapsulated CsPbI<sub>3</sub> films freshly prepared and aged for 60 days.

and chemical stability of CsPbI<sub>3</sub> perovskites. Although DMA cations could be completely removed once perovskite films are annealed at elevated temperature for an adequately long time,<sup>17</sup> special attention has to be paid regarding the actual chemical composition of the assumed all-inorganic CsPbI<sub>3</sub> because of the unanticipated DMA cations.<sup>7,13,15,27,29–32</sup>

Quantum dot/nanocrystal effects, by significantly reducing the grain size of perovskites to tens of nanometers or even smaller, are also widely applied to stabilize black-phase CsPbI<sub>3</sub>. This can be implemented by either synthesizing quantum dots (QDs) or doping perovskites with a small amount of organic ligands.<sup>19,33</sup> However, both the substantially increased grain boundary density arising from tiny grain size and insulating organic substances, like alkyl chains introduced during synthesis process, are detrimental for obtaining high-performance photovoltaic devices.

Alternatively, tuning the tolerance factor of CsPbI<sub>3</sub> to the stable region (0.81–1.11) is both theoretically and practically viable. However, the most commonly reported halide substitution by replacing I<sup>−</sup> with smaller Br<sup>−</sup> anion trades off the light-harvesting ability of CsPbI<sub>3</sub> because of the broadening of the bandgap.<sup>22</sup> Introducing quasi-2D or 2D perovskite capping layers to form 2D/3D heterojunctions has been reported to improve the phase stability of CsPbI<sub>3</sub> perovskites effectively.<sup>26,27</sup> However, the 2D perovskites incorporated may hinder the carrier transport, thus lowering their efficiency.<sup>14</sup> Therefore, it remains a crucial challenge to realize both the stabilization of the black phase of CsPbI<sub>3</sub> and superior performance of its photovoltaic devices simultaneously.

Here, we introduce a facile mediator–antisolvent strategy (MAS) combining PCBM/CBZ mixed antisolvent and MAI mediator to prepare stable black-phase CsPbI<sub>3</sub> films. Specifically, the use of PCBM/CBZ antisolvent decreases CsPbI<sub>3</sub> crystallite to a moderate size of ~200 nm, limiting the

quantity of grain boundaries. In addition, a judicious amount of MAI added in the precursor further improves the quality of CsPbI<sub>3</sub> films without enlarging the perovskite grains. The added MAI is eventually expelled at the high annealing temperature of 340 °C. The all inorganic solar cells achieve a PCE of ≥16%, which is among the highest efficiencies reported to date, and are stable with 95% of the initial PCE retained over 1000 h.

Figure 1a shows schematics of the MAS method. In detail, PCBM/CBZ antisolvent was applied to prepare perovskite films during the spin-coating process. Perovskite precursor was prepared by dissolving equal molar amounts of CsI and PbI<sub>2</sub> in DMF with 2% MAI (molar ratio to CsI) added. After annealing at 340 °C for 3 min, dark brown perovskite films with mirror-like surface were obtained. In addition, a reference sample was prepared by a traditional one-step method.<sup>7</sup> Compared with MAS, in the traditional one-step method neither MAI additives nor antisolvent was applied.

The perovskite films fabricated by MAS are far more stable in ambient air than the reference sample. After exposure to air for 30 min, there was little change in color for the film fabricated by MAS (Figure 1b), while the reference sample quickly turned yellow within 5 min. Figure 1c shows XRD data of CsPbI<sub>3</sub> films prepared with MAS or conventional one-step method, with both films encapsulated with Kapton tape. For both films, a gentle background diffraction ridge associated with the Kapton tape centered at about 18° is observed. For the film prepared with MAS, the diffraction peaks at  $2\theta = 14.4^\circ$ ,  $20.6^\circ$ , and  $28.9^\circ$  correspond to (100), (110), and (200) crystal planes of black-phase CsPbI<sub>3</sub> perovskites, respectively. However, the film prepared with the conventional one-step method degraded before the XRD test even after careful encapsulation. The measured XRD pattern identifies it as  $\delta$ -CsPbI<sub>3</sub>. Moreover, after being encapsulated with glass slides

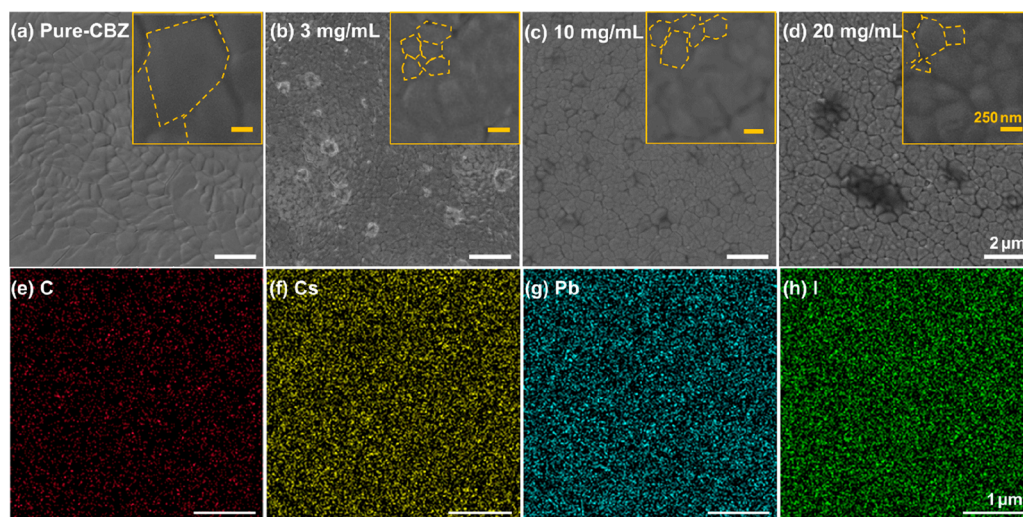


**Figure 2.** Top-view SEM and EDX images of the  $\text{CsPbI}_3$  films treated with various antisolvents. SEM images of perovskite films treated with PCBM/CBZ antisolvents with various concentrations: (a) pure-CBZ, (b) 3 mg/mL, (c) 10 mg/mL, and (d) 20 mg/mL. The scale bars are 2  $\mu\text{m}$ . Insets are magnified images with a scale bar of 250 nm. Element distribution of  $\text{CsPbI}_3$  films treated with 3 mg/mL PCBM/CBZ antisolvent, including (e) C, (f) Cs, (g) Pb, and (h) I. The scale bars are 1  $\mu\text{m}$ .

using UV glue, black-phase  $\text{CsPbI}_3$  prepared with MAS is preserved over 2 months when kept in ambient air with 70%–90% relative humidity as suggested by absorption spectra (shown in Figure 1d). It is noted that no HI/HPbI<sub>3</sub> or DMAI is used to prepare perovskite precursor in MAS and the thermal annealing temperature (340 °C) is high enough, so that the possibility of introducing  $\text{Cs}_{1-x}\text{DMA}_x\text{PbI}_3$  is excluded.

Next we investigated the role of PCBM and MAI in the formation of the stable  $\text{CsPbI}_3$  films. First, the influence of PCBM dissolved in antisolvent (CBZ) is investigated. In this case, perovskite precursor solution was prepared by dissolving 0.625 mmol of CsI and  $\text{PbI}_2$  in 1 mL of DMF without adding MAI. We used scanning electron microscopy (SEM) to investigate the surface morphologies of perovskite films treated with various PCBM/CBZ solutions (pure CBZ, 3 mg/mL, 10 mg/mL, and 20 mg/mL).

It is found that the  $\text{CsPbI}_3$  film treated with pure CBZ has an average grain size of about 800 nm, as shown in Figure 2a. For the films treated with 3 mg/mL PCBM/CBZ antisolvent, the grain size substantially decreases to an average value of  $\sim 200$  nm (Figure 2b). As the concentration increases to 10 or 20 mg/mL, micrometer-sized grains appear, which are composed of a number of small grains of around 200 nm in size. Meanwhile, big dark dots appear which could be ascribed to aggregation of PCBM. It is also found that the  $\text{CsPbI}_3$  film prepared with no antisolvent applied during the spin-coating process exhibits grain size and morphology similar to those of the film treated with pure CBZ (Figure S1). These results lead to a conclusion that it is PCBM, rather than CBZ, that is responsible for the decrease of perovskite grain size. Atomic force microscopy (AFM) was further performed to compare surface roughness of the perovskite films treated with different PCBM/CBZ antisolvents (3, 10, and 20 mg/mL). As depicted in Figure S2, root-mean square (RMS) roughness of the perovskite films treated with 3 mg/mL PCBM/CBZ, 10 mg/mL PCBM/CBZ, and 20 mg/mL PCBM/CBZ are 12.4, 17.1, and 26.3 nm, respectively. The AFM results demonstrate that the surface of perovskite films treated with 3 mg/mL PCBM/CBZ is smoothest, which is consistent with the observation of SEM imaging. Figure S3 shows these perovskite films show

similar absorption profiles with a consistent absorption edge at around 720 nm (1.73 eV). Nevertheless,  $\text{CsPbI}_3$  films treated with 3 mg/mL PCBM/CBZ antisolvent shows the strongest absorbance compared with other samples, which is ascribed to its smoother morphology. In addition, the element distribution of  $\text{CsPbI}_3$  films treated with 3 mg/mL PCBM/CBZ antisolvent was measured by energy-dispersive X-ray spectroscopy (EDX) mapping. The EDX images (Figure 2f–h) indicate Cs, Pb, and I are uniformly distributed without apparent segregation or aggregation. As shown in Figure 2e, C is sparsely distributed and is considered to represent PCBM. Furthermore, inorganic PSCs were fabricated based on these PCBM/CBZ-treated perovskite films following a structure of ITO/ $\text{SnO}_2$ / $\text{CsPbI}_3$ /Spiro-OMeTAD/Au. The photovoltaic performance of the devices is shown in Table S1. Apparently, significant improvement for PCE is achieved via PCBM/CBZ treatment, from 10.6% for the best device treated with pure CBZ to 14.3% for the champion device treated with 3 mg/mL PCBM/CBZ. Although all of the photovoltaic parameters have been improved in PCBM-treated devices, the performance is still limited because of relatively low fill factor (FF) and open-circuit voltage ( $V_{oc}$ ).

Furthermore, MAI was added to the perovskite precursor with the expectation to enhance the quality of PCBM/CBZ-treated inorganic perovskite films. Precursors were prepared by adding various amounts of MAI (2%, 5%, 10%, and 15% of MAI, molar ratio to CsI in precursor) into a 0.625 M solution composed of equal molar ratio of CsI and  $\text{PbI}_2$  in DMF. It is noted that 3 mg/mL PCBM/CBZ antisolvent was applied during spin-coating in each case. The obtained perovskite film is referred to as  $x\%$  MAI- $\text{CsPbI}_3$  ( $x = 2, 5, 10, 15$ ). Figure S4 shows SEM images for 2%, 5%, 10% and 15% MAI- $\text{CsPbI}_3$  films. As shown in Figure S5, the average grain size for 2% MAI- $\text{CsPbI}_3$  film is 225 nm, showing negligible difference compared with that of perovskite films fabricated by only 3 mg/mL PCBM/CBZ treatment. With more MAI added (5%, 10%, 15%), perovskite grains grow larger as shown in Figure S4. For 15% MAI, the grain size is nearly 4  $\mu\text{m}$ , almost 20 times larger than that of 2% MAI- $\text{CsPbI}_3$  films. To stabilize the black phase, small grain size is preferred rather than larger

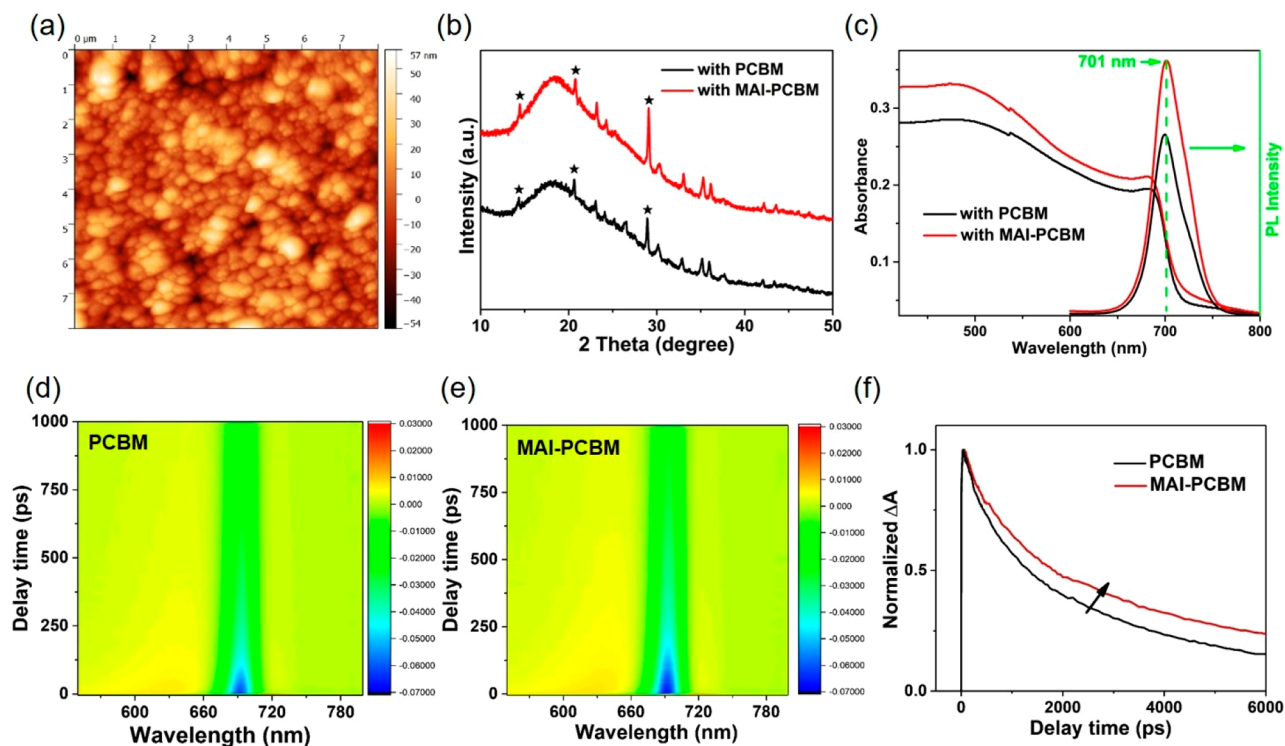


**Figure 3.** Characterizations of PCBM/CBZ-treated CsPbI<sub>3</sub> films prepared with or without MAI mediator added in precursors. (a) AFM image of CsPbI<sub>3</sub> films prepared with 2% MAI mediator. (b) XRD patterns, (c) absorption and PL spectra, (d and e) TAS response, and (f) TAS decay at 695 nm of CsPbI<sub>3</sub> films prepared with and without 2% MAI mediator.

grain size as its large surface-to-volume ratio would prevent the black phase from transitioning to yellow phase. As a result, adding 2% MAI was selected for enhancing film quality without trading off long-term stability. AFM image (Figure 3a) of the selected perovskite films has a RMS roughness of 10.6 nm in the range of  $8 \times 8 \mu\text{m}^2$ , reflecting a smoother surface by adding MAI additive. As shown in Figure 3b, XRD results demonstrate that 2% MAI-CsPbI<sub>3</sub> perovskite films, noted as MAI-PCBM in figures, show the same crystalline structure but better crystallinity compared with 0% MAI-CsPbI<sub>3</sub> perovskite films (noted as PCBM in figures). In addition, the ratios of diffraction peak (P)  $28.9^\circ$  to  $20.6^\circ$ , namely,  $P_{28.9^\circ}/P_{20.6^\circ}$ , are calculated to be 3.3 and 2 for 2% MAI-CsPbI<sub>3</sub> and 0% MAI-CsPbI<sub>3</sub>, respectively. This indicates that the perovskite film grows preferentially with (200) facet on adding MAI. It should be noted that no additional peaks associated with MAPbI<sub>3</sub> structure is present, which suggests that the resultant perovskite film was completely converted to black-phase CsPbI<sub>3</sub>. Furthermore, quantitative analysis for elemental composition of the 2% MAI-CsPbI<sub>3</sub> film reveals an atomic ratio (%) of 17.73:21.38:60.89 for Cs:Pb:I (Figure S6), which is close to the ideal stoichiometric ratio of CsPbI<sub>3</sub>.

Figure 3c shows the ultraviolet–visible (UV–vis) absorption and steady-state photoluminescence (PL) spectra of 0% MAI-CsPbI<sub>3</sub> perovskite films and 2% MAI-CsPbI<sub>3</sub> perovskite films. Although both films show similar absorption profile with cutoff edge wavelength at around 720 nm, the MAI-mediated CsPbI<sub>3</sub> film shows higher absorption, which is beneficial for light harvesting and short-circuit current density ( $J_{\text{sc}}$ ) improvement. As determined from the Tauc plot (Figure S7), 2% MAI-CsPbI<sub>3</sub> perovskite films show an optical bandgap of 1.735 eV. The PL spectra, obtained from the characterization of perovskite films deposited on glass substrates, show that 2%

MAI-CsPbI<sub>3</sub> exhibits an identical emission center but higher emission intensity compared with its counterpart. Generally, this phenomenon could be ascribed to the depression of defect-induced recombination.<sup>19</sup> The stronger PL intensity demonstrates fewer traps and defects within the perovskite film, thus leading to more effective utilization of photoinduced charge carriers and enhancement of device performance.

To further study the photocarrier dynamics of the 0% and 2% MAI-CsPbI<sub>3</sub> films, we carried out measurements of transient absorption spectroscopy (TAS) and time-resolved photoluminescence (TRPL), as shown in Figures 3d,e and S8, respectively. For both films, as can be seen from Figure 3d,e, the ground-state bleaching (GSB) is located at around 695 nm, which is close to the absorption edge and PL emission center. As shown in Figure 3f, decay curves abstracted from the TAS results (wavelength is set at 695 nm) show that the 2% MAI-CsPbI<sub>3</sub> film has a slower feature than that of the 0% MAI-CsPbI<sub>3</sub> perovskite film. TRPL measurements (Figure S8) on perovskite films deposited on glass substrates also show the 2% MAI-mediated CsPbI<sub>3</sub> film possesses a slower decay behavior. When the curves were fit to a biexponential function, defect-induced nonradiative recombination lifetime ( $\tau_1$ ) and radiative recombination lifetime ( $\tau_2$ ) were extracted, and they are listed in the inset of Figure S8.<sup>4</sup> The radiative recombination lifetime for CsPbI<sub>3</sub> films increased from 8.8 to 10.8 ns through the use of MAI additive, suggesting defects or traps have been suppressed. Besides, as listed in Figure S8, the ratio of  $A_2/A_1$  for MAI-PCBM perovskites (4.3) is almost twice that of PCBM perovskites (2.1), which reveals that the nonradiative recombination channel is depressed. Furthermore, TAS was tested for investigating carrier transport at interfaces of SnO<sub>2</sub>/perovskites (Figure S9) and perovskites/Spiro-OMeTAD (Figure S10). Both films show quenching behavior, but the

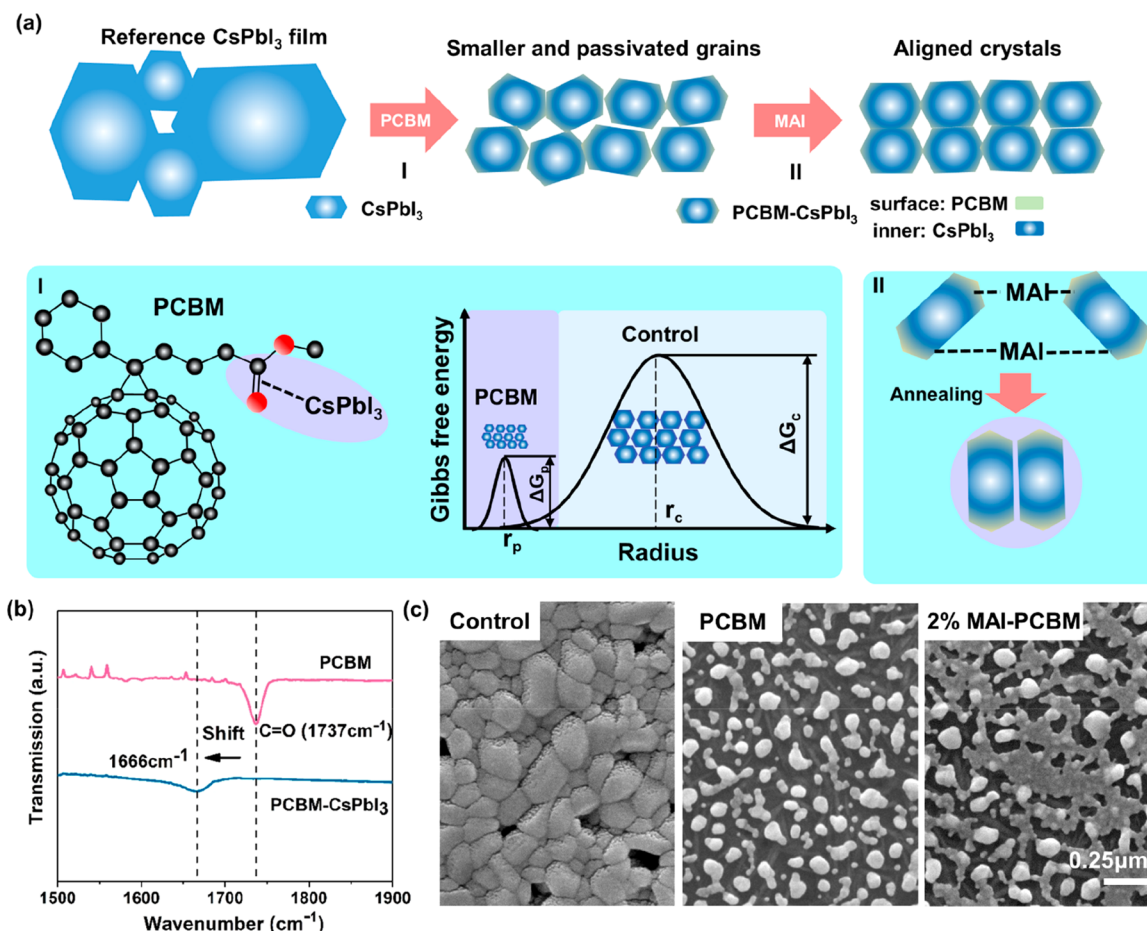


**Figure 4.** Crystallization process of CsPbI<sub>3</sub> films prepared with MAS. (a) Proposed mechanism of MAS. PCBM-CsPbI<sub>3</sub> represents CsPbI<sub>3</sub> grains surrounded by PCBM molecules; “I” and “II” represent the effects of PCBM and MAI on CsPbI<sub>3</sub> films, respectively. (b) FTIR spectra of PCBM and PCBM-treated CsPbI<sub>3</sub> (PCBM-CsPbI<sub>3</sub>). (c) SEM images of spin-coated perovskite films (without annealing) prepared from different perovskite precursors. For control sample, the film was prepared via the traditional one-step method.

2% MAI-CsPbI<sub>3</sub> film exhibits shorter lifetime, which indicates improved carrier extraction ability at the interfaces. Confocal laser scanning fluorescence microscopy (CLSM) results (Figure S11), which can identify distribution of emissive chemical composition by taking advantage of the differences in their emission spectra, suggest the perovskite film formed by adding 2% MAI is more uniform. It is noted the emission, highlighted in red, collected between 700 and 800 nm is attributed to CsPbI<sub>3</sub> perovskite. In conclusion, the perovskite film achieved enhanced quality in terms of crystallinity, morphology, and optoelectronic properties by adding MAI additive.

We further investigated the mechanism of MAS by revealing how PCBM and MAI influence the crystallization process of CsPbI<sub>3</sub> films. As shown in Figure 4a, our proposed mechanism shows that the function of MAS can be divided into two aspects: the functions of PCBM (I) and MAI (II) are primarily reducing grain size and aligning crystals, respectively.

Obviously, the grain size of CsPbI<sub>3</sub> films is greatly decreased once PCBM is applied, as can be seen from Figures 2 and S1. It is noted that this phenomenon is very different from what is reported when PCBM is doped in organic–inorganic hybrid perovskites, where larger perovskite grains are obtained.<sup>34–36</sup> This implies PCBM has different effects during the crystallization process of inorganic perovskites. A smaller grain size contributes to stabilizing the black phase of CsPbI<sub>3</sub>

as the high surface energy can act as a pause to the thermodynamically favored degradation process from the black phase to yellow phase.<sup>18,31</sup> Meanwhile, PCBM/CBZ antisolvent with higher concentration leads to rougher film morphologies as shown in Figures 2 and S2. This originates from the interaction between CsPbI<sub>3</sub> and PCBM, as demonstrated by Fourier-transform infrared spectroscopy (FTIR) measurements (Figure 4b). As shown in Figure 4b, the FTIR spectrum of PCBM possesses a peak located at 1737 cm<sup>-1</sup>, which is attributed to stretching vibration of the C=O group. When PCBM is blended with CsPbI<sub>3</sub>, the characteristic peak of PCBM shifted from 1737 to 1666 cm<sup>-1</sup>, which is attributed to the bonding between the C=O group of the PCBM molecule and CsPbI<sub>3</sub>. Such bonding originates from electrostatic attraction between the polar group and charged particles. Here, Cs<sup>+</sup> of CsPbI<sub>3</sub> tends to interact with oxygen of C=O, through which PCBM molecules eventually anchor on grown CsPbI<sub>3</sub> grains. Therefore, a charge interface between CsPbI<sub>3</sub> and PCBM can be expected which increases charge density at the grain surface and lowers surface tension of CsPbI<sub>3</sub> grains.<sup>37,38</sup> This plays a crucial role in the initial crystallization stage of CsPbI<sub>3</sub> films as it would lower the critical Gibbs free energy ( $\Delta G$ ) for nucleation as well as critical nuclei size ( $r$ ), as depicted in Figure 4a.<sup>4,20</sup> During the crystallization process of CsPbI<sub>3</sub>, because nuclei can stabilize at a smaller size  $r_p$ , the grain size of CsPbI<sub>3</sub> films would be

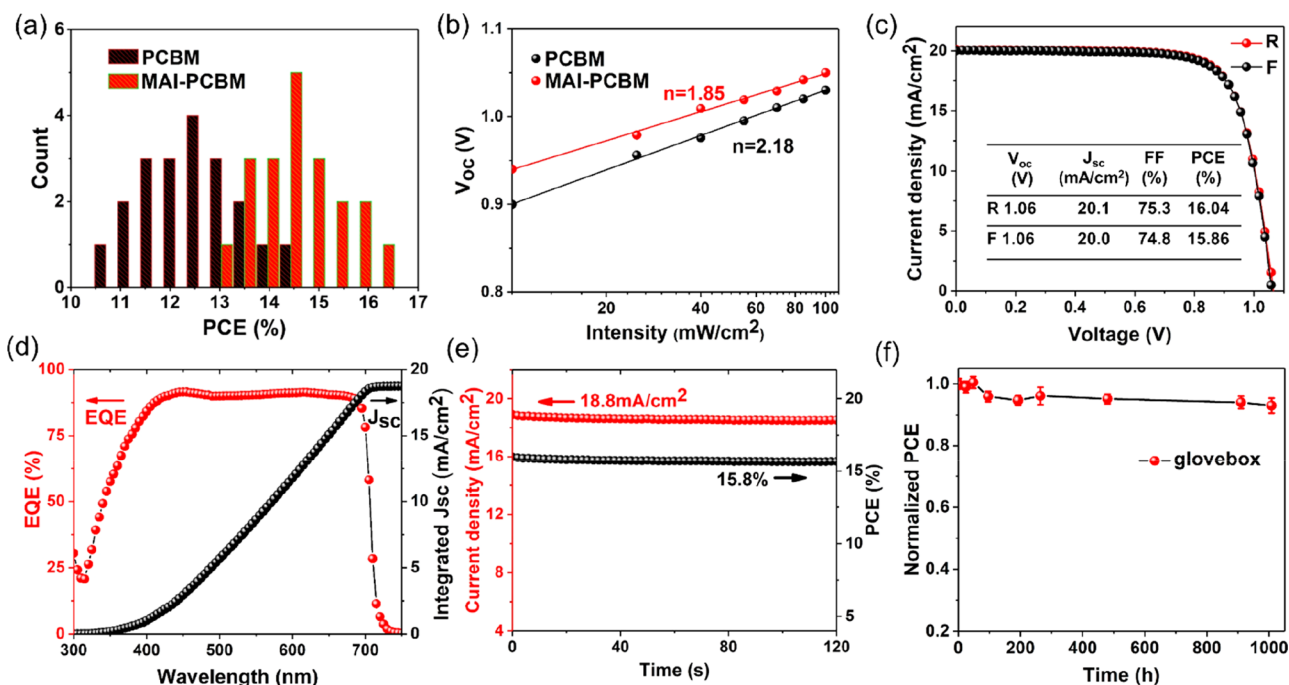


Figure 5. Performance of  $\text{CsPbI}_3$  solar cells. (a) PCE distributions and (b) dependence of  $V_{oc}$  on light intensity of PSCs based on 0% MAI- $\text{CsPbI}_3$  (denoted as PCBM) and 2% MAI- $\text{CsPbI}_3$  (denoted as MAI-PCBM). (c)  $J$ - $V$  curves, (d) EQE and integrated current density, and (e) maximum power point tracking of the champion 2% MAI- $\text{CsPbI}_3$  device. (f) Stability of unencapsulated 2% MAI- $\text{CsPbI}_3$  PSCs prepared with MAS kept in an  $\text{N}_2$  glovebox for 1000 h.

substantially smaller as PCBM is applied because of a decrease of the critical Gibbs free energy ( $\Delta G_p$ ). In contrast, if the conventional one-step method is applied, the critical Gibbs free energy ( $\Delta G_c$ ) and critical nuclei size ( $r_c$ ) are much larger. As shown in Figure S12, thermogravimetric analysis (TGA) measurements show a negligible weight loss for PCBM at temperatures less than 400 °C, indicating that PCBM would not decompose at the annealing temperature we used. This is in agreement with previous work that reported the degradation temperature of PCBM is around 398 °C.<sup>39</sup> The slight weight loss (less than 1%) at around 280 °C for PCBM is ascribed to impurity sublimation.<sup>39</sup> Noting that the glass transition of PCBM is reported to be around 120 °C,<sup>40</sup> once cooled from the annealing temperature of 340 °C, PCBM molecules would introduce extra stress at the surface of  $\text{CsPbI}_3$  grains, thus facilitating the phase stabilization of black  $\text{CsPbI}_3$  thermodynamically.<sup>41</sup> However, the concentration for PCBM/CBZ should be optimized as higher concentration leads to aggregation of PCBM molecules so that the morphology of the obtained  $\text{CsPbI}_3$  films is damaged. In addition, we speculate that oxygen of the C=O group may fill the position of the  $\Gamma$  vacancy at the grain surface and cooperate with the Pb atom so that the defects of  $\text{CsPbI}_3$  films are passivated.<sup>33,42–45</sup> This would suppress photocarrier non-radiative recombination. In comparison with those  $\text{CsPbI}_3$  films obtained by dimensional engineering of which grains are tens of nanometers in size, our films composed of  $\sim 200$  nm grains introduce less grain boundary, and thus, it is beneficial for carrier transport.

On the other hand, MAI, which is added in the precursor, exhibits its influence in two ways. First, as shown in Figure S13, dynamic light scattering (DLS) measurements show that the average particle size of the  $\text{CsPbI}_3$  precursor is greatly decreased as MAI is added. This means MAI increases the

solubility of  $\text{CsPbI}_3$  in DMF, which is beneficial for obtaining thicker perovskite absorber layers. It is noted that the concentration of perovskite precursors for DLS measurements was slightly greater than the solubility limit to clearly show the contrast of the particle size in precursors with and without MAI additives. Second, MAI forms an intermediate with the other substances in the precursor. As shown in Figure S14, when the molar ratio of MAI increased up to 10%, the perovskite film became brown after PCBM/CBZ antisolvent was applied during the spin-coating process. As depicted in Figures 4c and S15, SEM measurements show that higher content of MAI results in denser morphology of the obtained perovskite films without annealing. A reasonable explanation is that  $\text{MAPbI}_3$  is formed through the coordination between MAI and  $\text{PbI}_2$  at boundaries of PCBM-surrounded  $\text{CsPbI}_3$  grains (noted as PCBM- $\text{CsPbI}_3$ ). Without MAI, PCBM- $\text{CsPbI}_3$  grains are randomly assembled because of the big molecule of PCBM, as evidenced by the less satisfactory morphology of PCBM-treated perovskite films shown in Figures 2 and S2. MAI at the grain boundaries would stitch adjacent PCBM- $\text{CsPbI}_3$  grains through  $\text{PbI}_2$ -MAI- $\text{PbI}_2$  interaction so that the obtained PCBM- $\text{CsPbI}_3$  grains stack in a more aligned manner. The enhanced crystallinity of perovskite films prepared with 2% MAI mediator shown in Figure 3b can serve as supportive evidence. It is known that the cations of  $\text{MAPbI}_3$  would degrade into gases when exposed to high temperature.<sup>46–48</sup> This is further confirmed by TGA characterization (Figure S12), which shows MAI starts to lose weight at 150 °C and completely decomposes at around 330 °C. Because the higher annealing temperature (340 °C) for perovskite films is adopted, it is concluded that the added MAI contributes to form a temporary dark intermediate but eventually does not exist in the annealed  $\text{CsPbI}_3$  films. This is supported by the

XRD results shown in Figure 3b, as no diffraction peaks belonging to MAPbI<sub>3</sub> present.

We employed these CsPbI<sub>3</sub> perovskite films as light-absorbing layers to fabricate planar solar cells. Figure 5a shows PCE distributions of PSCs based on 0% MAI-CsPbI<sub>3</sub> and 2% MAI-CsPbI<sub>3</sub> perovskite films. The CsPbI<sub>3</sub> PSCs fabricated by combining PCBM/CBZ antisolvent treatment with MAI additive exhibit better performance compared with those based on only PCBM/CBZ antisolvent treatment. Detailed photovoltaic parameters are listed in Table S2. The dependence of  $V_{oc}$  on illumination intensity is compared in Figure 5b. For p–n junction solar cells, the relationship between  $V_{oc}$  and light intensity ( $I_n$ ) can be simplified as  $qV_{oc} = nkT_c \ln I_n$ , where  $q$ ,  $n$ ,  $k$ , and  $T_c$  represent elementary charge, ideality factor, Boltzmann constant, and temperature, respectively.<sup>49</sup> Ideality factor reflects the quality of a p–n junction. A value close to unity represents an ideal junction while a larger one means more nonradiative recombination channels present. For  $T = 300$  K, fitting the slope of lines plotted in Figure 5b yields  $n = 1.85$  and  $n = 2.18$  for solar cells based on 2% MAI-CsPbI<sub>3</sub> and 0% MAI-CsPbI<sub>3</sub> perovskite films, respectively. The ideality factor  $n = 1.85$  measured for the modified device is close to a hybrid perovskite solar cell as reported,<sup>49</sup> which demonstrates the beneficial influence of adding MAI.<sup>15</sup> For PCBM/CBZ antisolvent treatment, the best PCE of the devices is 14.34% with a  $V_{oc}$  of 0.99 eV,  $J_{sc}$  of 19.99 mA/cm<sup>2</sup>, and FF of 72.16%, as shown in Figure S16. In contrast, the best device (Figure 5c) prepared with both MAI additive and PCBM/CBZ antisolvent achieves a champion PCE of 16.04% with the  $V_{oc}$  of 1.06 V,  $J_{sc}$  of 20.1 mA/cm<sup>2</sup>, and FF of 75.3% under reverse voltage scan. A PCE of 15.86% is obtained under forward scan, indicating negligible hysteresis. As shown in Table S3, compared with other reported CsPbI<sub>3</sub> PSCs, the efficiency of our devices is among the highest.

The external quantum efficiency (EQE) spectrum shown in Figure 5d exhibits high value over 85% in the wavelength range from ~400 to ~670 nm. The integrated current density of 19.2 mA/cm<sup>2</sup> is very close to the  $J_{sc}$  shown in the  $J$ – $V$  curves. A stabilized efficiency of 15.8% with current density of 18.8 mA/cm<sup>2</sup> is recorded by tracking the maximum power point, as displayed in Figure 5e. Furthermore, the solar cells based on 2% MAI-CsPbI<sub>3</sub> can retain 95% of their original efficiency after aging in a nitrogen glovebox for 1000 h, as depicted in Figure 5f. The outstanding performance of our devices in terms of PCE and long-term stability demonstrates that the strategy yielding a moderate grain size of crystallite and suitable coordination is an effective way to stabilize the black phase without sacrificing its superior optoelectronic properties. Coordination substances with better charge transportation that would facilitate carrier extraction and collection will be explored in the next stage of the work.

To conclude, we demonstrated a MAS strategy to fabricate stable and efficient CsPbI<sub>3</sub> solar cells without introducing HI or HPbI<sub>3</sub> in the perovskite precursor. As a result, dispute on whether the obtained perovskite is pure inorganic or an organic–inorganic hybrid is avoided. When the PCBM/CBZ antisolvent is applied during the spin-coating process, the grain size of CsPbI<sub>3</sub> is substantially decreased from micrometer to ~200 nm, which is beneficial for both the stabilization of black-phase CsPbI<sub>3</sub> and charge transport. Furthermore, MAI additive is applied to improve the quality of PCBM-treated CsPbI<sub>3</sub> films without introducing organic cations in the final films. Based on this strategy, CsPbI<sub>3</sub> solar cells were fabricated and

showed a champion PCE of 16.04%. In addition, the devices showed superior storage stability, and 95% of the initial PCE was retained over a period of 1000 h. With further optimization of device energy level alignment, surface passivation, and composition tuning of perovskites, highly efficient and stable inorganic perovskite solar cells can be expected. Our work provides a new way to balance the stability and optoelectronic properties of black-phase CsPbI<sub>3</sub>, which would inform more work exploring efficient and stable CsPbI<sub>3</sub> perovskite solar cells as well as other opto-electrical devices.

## ■ ASSOCIATED CONTENT

### Supporting Information

The Supporting Information is available free of charge at <https://pubs.acs.org/doi/10.1021/acsnenergylett.0c00497>.

Experimental methods, characterizations of films and devices (optical and electron microscopy images, EDX results, carrier dynamics measurements, TGA results, DLS data, and  $J$ – $V$  curves), device performance statistics, and performance comparison (PDF)

## ■ AUTHOR INFORMATION

### Corresponding Authors

**Feng Wang** – School of Optoelectronic Science and Engineering, University of Electronic Science and Technology of China, Chengdu, Sichuan 610054, China; Beijing Key Laboratory for Theory and Technology of Advanced Battery Materials, Key Laboratory of Polymer Chemistry and Physics of Ministry of Education, BIC-ESAT, Department of Materials Science and Engineering, College of Engineering, Peking University, Beijing 100871, China; [orcid.org/0000-0001-7626-3112](https://orcid.org/0000-0001-7626-3112); Email: [wangfeeng1990@gmail.com](mailto:wangfeeng1990@gmail.com)

**Shibin Li** – School of Optoelectronic Science and Engineering, University of Electronic Science and Technology of China, Chengdu, Sichuan 610054, China; [orcid.org/0000-0002-0591-5491](https://orcid.org/0000-0002-0591-5491); Email: [shibinli@uestc.edu.cn](mailto:shibinli@uestc.edu.cn)

### Authors

**Ting Zhang** – School of Optoelectronic Science and Engineering, University of Electronic Science and Technology of China, Chengdu, Sichuan 610054, China; Department of Physics, Department of Chemistry, and JILA, University of Colorado, Boulder, Colorado 80309, United States

**Hao Chen** – School of Optoelectronic Science and Engineering, University of Electronic Science and Technology of China, Chengdu, Sichuan 610054, China

**Long Ji** – School of Optoelectronic Science and Engineering, University of Electronic Science and Technology of China, Chengdu, Sichuan 610054, China

**Yafei Wang** – School of Optoelectronic Science and Engineering, University of Electronic Science and Technology of China, Chengdu, Sichuan 610054, China

**Chun Li** – School of Optoelectronic Science and Engineering, University of Electronic Science and Technology of China, Chengdu, Sichuan 610054, China; [orcid.org/0000-0002-8190-9843](https://orcid.org/0000-0002-8190-9843)

**Markus B. Raschke** – Department of Physics, Department of Chemistry, and JILA, University of Colorado, Boulder, Colorado 80309, United States; [orcid.org/0000-0003-2822-851X](https://orcid.org/0000-0003-2822-851X)

Complete contact information is available at:

<https://pubs.acs.org/doi/10.1021/acsnenergylett.0c00497>

## Notes

The authors declare no competing financial interest.

## ACKNOWLEDGMENTS

This work was supported by the National Natural Science Foundation of China (61874150), the Sichuan Key Project for Applied Fundamental Research (20YYJC4341) and the Key Laboratory Foundation of Chinese Academy of Sciences (2019LBC). This work was also partially supported by University of Colorado, Boulder and Peking University.

## REFERENCES

- (1) Kojima, A.; Teshima, K.; Shirai, Y.; Miyasaka, T. Organometal halide perovskites as visible-light sensitizers for photovoltaic cells. *J. Am. Chem. Soc.* **2009**, *131*, 6050–6051.
- (2) NREL. Best research-cell efficiencies chart. <http://www.nrel.gov/pv/cell-efficiency.html> (accessed 2019-04).
- (3) Correa-Baena, J.-P.; Abate, A.; Saliba, M.; Tress, W.; Jacobsson, T. J.; Grätzel, M.; Hagfeldt, A. The rapid evolution of highly efficient perovskite solar cells. *Energy Environ. Sci.* **2017**, *10*, 710–727.
- (4) Wang, F.; Zhang, T.; Wang, Y.; Liu, D.; Zhang, P.; Chen, H.; Ji, L.; Chen, L.; Chen, Z. D.; Wu, J.; Liu, X.; Li, Y.; Li, S. Steering the crystallization of perovskites for high-performance solar cells in ambient air. *J. Mater. Chem. A* **2019**, *7*, 12166–12175.
- (5) Ji, L.; Zhang, X.; Zhang, T.; Wang, Y.; Wang, F.; Zhong, Z.; Chen, Z. D.; Xiao, Z.; Chen, L.; Li, S. Band alignment of Pb-Sn mixed triple cation perovskites for inverted solar cells with negligible hysteresis. *J. Mater. Chem. A* **2019**, *7*, 9154–9162.
- (6) Chen, H.; Xiang, S.; Li, W.; Liu, H.; Zhu, L.; Yang, S. Inorganic perovskite solar cells: a rapidly growing field. *Solar RRL* **2018**, *2*, 1700188.
- (7) Eperon, G. E.; Paterno, G. M.; Sutton, R. J.; Zampetti, A.; Haghighirad, A. A.; Cacialli, F.; Snaith, H. J. Inorganic caesium lead iodide perovskite solar cells. *J. Mater. Chem. A* **2015**, *3*, 19688–19695.
- (8) Dastidar, S.; Hawley, C. J.; Dillon, A. D.; Gutierrez-Perez, A. D.; Spanier, J. E.; Fafarman, A. T. Quantitative phase-change thermodynamics and metastability of perovskite-phase cesium lead iodide. *J. Phys. Chem. Lett.* **2017**, *8*, 1278–1282.
- (9) Dastidar, S.; Egger, D. A.; Tan, L. Z.; Cromer, S. B.; Dillon, A. D.; Liu, S.; Kronik, L.; Rappe, A. M.; Fafarman, A. T. High chloride doping levels stabilize the perovskite phase of cesium lead iodide. *Nano Lett.* **2016**, *16*, 3563–3570.
- (10) Jiang, Y.; Yuan, J.; Ni, Y.; Yang, J.; Wang, Y.; Jiu, T.; Yuan, M.; Chen, J. Reduced-dimensional  $\alpha$ -CsPbX<sub>3</sub> perovskites for efficient and stable photovoltaics. *Joule* **2018**, *2*, 1356–1368.
- (11) Sutton, R. J.; Filip, M. R.; Haghighirad, A. A.; Sakai, N.; Wenger, B.; Giustino, F.; Snaith, H. J. Cubic or orthorhombic? Revealing the crystal structure of metastable black-phase CsPbI<sub>3</sub> by theory and experiment. *ACS Energy Lett.* **2018**, *3*, 1787–1794.
- (12) Marronnier, A.; Roma, G.; Boyer-Richard, S.; Pedesseau, L.; Jancu, J.-M.; Bonnassieux, Y.; Katan, C.; Stoumpos, C. C.; Kanatzidis, M. G.; Even, J. Anharmonicity and disorder in the black phases of cesium lead iodide used for stable inorganic perovskite solar cells. *ACS Nano* **2018**, *12*, 3477–3486.
- (13) Zhao, B.; Jin, S. F.; Huang, S.; Liu, N.; Ma, J. Y.; Xue, D. J.; Han, Q.; Ding, J.; Ge, Q. Q.; Feng, Y.; Hu, J. S. Thermodynamically stable orthorhombic  $\gamma$ -CsPbI<sub>3</sub> thin films for high-performance photovoltaics. *J. Am. Chem. Soc.* **2018**, *140*, 11716–11725.
- (14) Wang, Y.; Zhang, T.; Kan, M.; Zhao, Y. Bifunctional stabilization of all-inorganic  $\alpha$ -CsPbI<sub>3</sub> perovskite for 17% efficiency photovoltaics. *J. Am. Chem. Soc.* **2018**, *140*, 12345–12348.
- (15) Wang, K.; Jin, Z.; Liang, L.; Bian, H.; Wang, H.; Feng, J.; Wang, Q.; Liu, S. Chlorine doping for black  $\gamma$ -CsPbI<sub>3</sub> solar cells with stabilized efficiency beyond 16%. *Nano Energy* **2019**, *58*, 175–182.
- (16) Wang, Y.; Dar, M. I.; Ono, L. K.; Zhang, T.; Kan, M.; Li, Y.; Zhang, L.; Wang, X.; Yang, Y.; Gao, X.; Qi, Y.; Grätzel, M.; Zhao, Y. Thermodynamically stabilized  $\beta$ -CsPbI<sub>3</sub>-based perovskite solar cells with efficiencies > 18%. *Science* **2019**, *365*, 591–595.
- (17) Wang, Y.; Liu, X.; Zhang, T.; Wang, X.; Kan, M.; Shi, J.; Zhao, Y. The role of dimethylammonium iodide in CsPbI<sub>3</sub> perovskite fabrication: additive or dopant? *Angew. Chem., Int. Ed.* **2019**, *58*, 16691–16696.
- (18) Swarnkar, A.; Marshall, A. R.; Sanehira, E. M.; Chernomordik, B. D.; Moore, D. T.; Christians, J. A.; Chakrabarti, T.; Luther, J. M. Quantum dot-induced phase stabilization of  $\alpha$ -CsPbI<sub>3</sub> perovskite for high-efficiency photovoltaics. *Science* **2016**, *354*, 92–95.
- (19) Ling, X.; Zhou, S.; Yuan, J.; Shi, J.; Qian, Y.; Larson, B. W.; Zhao, Q.; Qin, C.; Li, F.; Shi, G.; Stewart, C.; Hu, J.; Zhang, X.; Luther, J. M.; Duhm, S.; Ma, W. 14.1% CsPbI<sub>3</sub> perovskite quantum dot solar cells via cesium cation passivation. *Adv. Energy Mater.* **2019**, *9*, 1900721.
- (20) Wang, C.; Chesman, A. S. R.; Jasieniak, J. J. Stabilizing the cubic perovskite phase of CsPbI<sub>3</sub> nanocrystals by using an alkyl phosphonic acid. *Chem. Commun.* **2017**, *53*, 232–235.
- (21) Liang, L.; Liu, M.; Jin, Z.; Wang, Q.; Wang, H.; Bian, H.; Shi, F.; Liu, S. Optical management with nanoparticles for a light conversion efficiency enhancement in inorganic  $\gamma$ -CsPbI<sub>3</sub> solar cells. *Nano Lett.* **2019**, *19*, 1796–1804.
- (22) Chen, W.; Chen, H.; Xu, G.; Xue, R.; Wang, S.; Li, Y.; Li, Y. Precise control of crystal growth for highly efficient CsPbI<sub>2</sub>Br perovskite solar cells. *Joule* **2019**, *3*, 191–204.
- (23) Shao, Z.; Wang, Z.; Li, Z.; Fan, Y.; Meng, H.; Liu, R.; Wang, Y.; Hagfeldt, A.; Cui, G.; Pang, S. A scalable methylamine gas healing strategy for high-efficiency inorganic perovskite solar cells. *Angew. Chem., Int. Ed.* **2019**, *58*, 5587–5591.
- (24) Nam, J. K.; Chai, S. U.; Cha, W.; Choi, Y. J.; Kim, W.; Jung, M. S.; Kwon, J.; Kim, D.; Park, J. H. Potassium incorporation for enhanced performance and stability of fully inorganic cesium lead halide perovskite solar cells. *Nano Lett.* **2017**, *17*, 2028–2033.
- (25) Hu, Y.; Bai, F.; Liu, X.; Ji, Q.; Miao, X.; Qiu, T.; Zhang, S. Bismuth incorporation stabilized  $\alpha$ -CsPbI<sub>3</sub> for fully inorganic perovskite solar cells. *ACS Energy Lett.* **2017**, *2*, 2219–2227.
- (26) Zhang, T.; Dar, M. I.; Li, G.; Xu, F.; Guo, N.; Grätzel, M.; Zhao, Y. Bication lead iodide 2D perovskite component to stabilize inorganic  $\alpha$ -CsPbI<sub>3</sub> perovskite phase for high-efficiency solar cells. *Sci. Adv.* **2017**, *3*, No. e1700841.
- (27) Wang, Y.; Zhang, T.; Kan, M.; Li, Y.; Wang, T.; Zhao, Y. Efficient  $\alpha$ -CsPbI<sub>3</sub> photovoltaics with surface terminated organic cations. *Joule* **2018**, *2*, 2065–2075.
- (28) Ke, W.; Spanopoulos, I.; Stoumpos, C. C.; Kanatzidis, M. G. Myths and reality of HPbI<sub>3</sub> in halide perovskite solar cells. *Nat. Commun.* **2018**, *9*, 4785.
- (29) Wang, K.; Jin, Z.; Liang, L.; Bian, H.; Bai, D.; Wang, H.; Zhang, J.; Wang, Q.; Liu, S. All-inorganic cesium lead iodide perovskite solar cells with stabilized efficiency beyond 15%. *Nat. Commun.* **2018**, *9*, 4544.
- (30) Xiang, S.; Fu, Z.; Li, W.; Wei, Y.; Liu, J.; Liu, H.; Zhu, L.; Zhang, R.; Chen, H. Highly air-stable carbon-based  $\alpha$ -CsPbI<sub>3</sub> perovskite solar cells with a broadened optical spectrum. *ACS Energy Lett.* **2018**, *3*, 1824–1831.
- (31) Haque, F.; Wright, M.; Mahmud, M. A.; Yi, H.; Wang, D.; Duan, L.; Xu, C.; Upama, M. B.; Uddin, A. Effects of hydroiodic acid concentration on the properties of CsPbI<sub>3</sub> perovskite solar cells. *ACS Omega* **2018**, *3*, 11937–11944.
- (32) Wu, T.; Wang, Y.; Dai, Z.; Cui, D.; Wang, T.; Meng, X.; Bi, E.; Yang, X.; Han, L. Efficient and stable CsPbI<sub>3</sub> solar cells via regulating lattice distortion with surface organic terminal groups. *Adv. Mater.* **2019**, *31*, 1900605.
- (33) Wang, Q.; Zheng, X.; Deng, Y.; Zhao, J.; Chen, Z.; Huang, J. Stabilizing the  $\alpha$ -phase of CsPbI<sub>3</sub> perovskite by sulfobetaine zwitterions in one-step spin-coating films. *Joule* **2017**, *1*, 371–382.
- (34) Chiang, C.-H.; Wu, C.-G. Bulk heterojunction perovskite-PCBM solar cells with high fill factor. *Nat. Photonics* **2016**, *10*, 196.
- (35) Zhang, F.; Shi, W.; Luo, J.; Pellet, N.; Yi, C.; Li, X.; Zhao, X.; Dennis, T. J. S.; Li, X.; Wang, S.; Xiao, Y.; Zakeeruddin, S. M.; Bi, D.; Grätzel, M. Isomer-pure bis-PCBM-assisted crystal engineering of

perovskite solar cells showing excellent efficiency and stability. *Adv. Mater.* **2017**, *29*, 1606806.

(36) Wu, Y.; Yang, X.; Chen, W.; Yue, Y.; Cai, M.; Xie, F.; Bi, E.; Islam, A.; Han, L. Perovskite solar cells with 18.21% efficiency and area over 1 cm<sup>2</sup> fabricated by heterojunction engineering. *Nat. Energy* **2016**, *1*, 16148.

(37) Li, B.; Zhang, Y.; Fu, L.; Yu, T.; Zhou, S.; Zhang, L.; Yin, L. Surface passivation engineering strategy to fully-inorganic cubic CsPbI<sub>3</sub> perovskites for high-performance solar cells. *Nat. Commun.* **2018**, *9*, 1076.

(38) Ummadisingu, A.; Steier, L.; Seo, J.-Y.; Matsui, T.; Abate, A.; Tress, W.; Grätzel, M. The effect of illumination on the formation of metal halide perovskite films. *Nature* **2017**, *545*, 208–212.

(39) Ngo, T. T.; Nguyen, D. N.; Nguyen, V. T. Glass transition of PCBM, P3HT and their blends in quenched state. *Adv. Nat. Sci.: Nanosci. Nanotechnol.* **2012**, *3*, 045001.

(40) Warman, J. M.; de Haas, M. P.; Anthopoulos, T. D.; de Leeuw, D. M. The negative effect of high-temperature annealing on charge-carrier lifetimes in microcrystalline PCBM. *Adv. Mater.* **2006**, *18*, 2294–2298.

(41) Steele, J. A.; Jin, H.; Dovgaliuk, I.; Berger, R. F.; Braeckvelt, T.; Yuan, H.; Martin, C.; Solano, E.; Lejaeghere, K.; Rogge, S. M. J.; Notebaert, C.; Vandezande, W.; Janssen, K. P. F.; Goderis, B.; Debroye, E.; Wang, Y.-K.; Dong, Y.; Ma, D.; Saidaminov, M.; Tan, H.; Lu, Z.; Dyadkin, V.; Chernyshov, D.; Speybroeck, V. V.; Sargent, E. H.; Hofkens, J.; Roeffaers, M. B. J. Thermal unequilibrium of strained black CsPbI<sub>3</sub> thin films. *Science* **2019**, *365*, 679–684.

(42) Yang, S.; Chen, S.; Mosconi, E.; Fang, Y.; Xiao, X.; Wang, C.; Zhou, Y.; Yu, Z.; Zhao, J.; Gao, Y.; Angelis, F. D.; Huang, J. Stabilizing halide perovskite surfaces for solar cell operation with wide-bandgap lead oxysalts. *Science* **2019**, *365*, 473–478.

(43) Ball, J. M.; Petrozza, A. Defects in perovskite-halides and their effects in solar cells. *Nat Energy* **2016**, *1*, 16149.

(44) Shao, Y.; Xiao, Z.; Bi, C.; Yuan, Y.; Huang, J. Origin and elimination of photocurrent hysteresis by fullerene passivation in CH<sub>3</sub>NH<sub>3</sub>PbI<sub>3</sub> planar heterojunction solar cells. *Nat. Commun.* **2014**, *5*, 5784.

(45) Wang, Q.; Shao, Y.; Dong, Q.; Xiao, Z.; Yuan, Y.; Huang, J. Large fill-factor bilayer iodine perovskite solar cells fabricated by a low-temperature solution-process. *Energy Environ. Sci.* **2014**, *7*, 2359–2365.

(46) Zhang, T.; Wang, Y.; Wang, X.; Wu, M.; Liu, W.; Zhao, Y. Organic salt mediated growth of phase pure and stable all-inorganic CsPbX<sub>3</sub> (X = I, Br) perovskites for efficient photovoltaics. *Sci. Bull.* **2019**, *64*, 1773–1779.

(47) Saliba, M.; Matsui, T.; Seo, J.-Y.; Domanski, K.; Correa-Baena, J.-P.; Nazeeruddin, M. K.; Zakeeruddin, S. M.; Tress, W.; Abate, A.; Hagfeldt, A.; Grätzel, M. Cesium-containing triple cation perovskite solar cells: improved stability, reproducibility and high efficiency. *Energy Environ. Sci.* **2016**, *9*, 1989–1997.

(48) Zhang, R.; Liu, D.; Wang, Y.; Zhang, T.; Gu, X.; Zhang, P.; Wu, J.; Chen, Z. D.; Zhao, Y.; Li, S. Theoretical lifetime extraction and experimental demonstration of stable cesium-containing tri-cation perovskite solar cells with high efficiency. *Electrochim. Acta* **2018**, *265*, 98–106.

(49) Singh, T.; Miyasaka, T. Stabilizing the efficiency beyond 20% with a mixed cation perovskite solar cells fabricated in ambient air under controlled humidity. *Adv. Energy Mater.* **2018**, *8*, 1700677.